Review Article **Open Access**

Johannes Kaschke* and Martin Wegener

Optical and Infrared Helical Metamaterials

DOI 10.1515/nanoph-2016-0005
Received October 26, 2015; accepted December 16, 2015

Abstract: By tailoring metamaterials with chiral unit cells, giant optical activity and strong circular dichroism have been achieved successfully over the past decade. Metamaterials based on arrays of metal helices have revolutionized the field of chiral metamaterials, because of their capability of exhibiting these pronounced chiro-optical effects over previously unmatched bandwidths.
More recently, a large number of new metamaterial designs based on metal helices have been introduced with either optimized optical performance or other chiro-optical properties for novel applications.
The fabrication of helical metamaterials is, however, challenging and even more so with growing complexity of the metamaterial designs. As conventional two-dimensional nanofabrication methods, for example, electron-beam lithography, are not well suited for helical metamaterials, the development of novel three-dimensional fabrication approaches has been triggered.
Here, we will discuss the theory for helical metamaterials and the principle of operation. We also review advancements in helical metamaterial design and their limitations and influence on optical performance. Furthermore, we will compare novel nano- and microfabrication techniques that have successfully yielded metallic helical metamaterials. Finally, we also discuss recently presented applications of helical metamaterials extending beyond the use of far-field circular polarizers.

Keywords: chiral metamaterials; circular polarization; plasmonics

1 Introduction

Over the past two decades, metamaterials have played a central role in nanophotonics. By designing a material with a periodic substructure on a subwavelength scale, the effective material parameters, for example, permittivity and permeability, can be tailored to meet one's desired application's criteria. Material parameters not found in nature, for example, a negative refractive index, can be realized, and with the help of metamaterials, new applications, such as light cloaking, have emerged [1]. Furthermore, as metamaterial designs are scalable, existing applications realized at wavelength regimes that have previously been difficult to access become possible. Past achievements and the status of current research has been discussed in Ref. [2].

One important subclass are chiral metamaterials (CMMs)—metamaterial unit cell designs with no plane of mirror symmetry. These CMMs can exhibit chiro-optical effects similar to that of circular dichroism or optical activity orders of magnitude larger than that found in natural materials. This is of particular importance for applications such as circular dichroism spectroscopy [3]. As most biological molecules are chiral, the two corresponding enantiomers can often solely be distinguished by their chiro-optical response, for example, their difference in absorption for left circularly polarized light (LCP) or right circularly polarized light (RCP). For visible frequencies, combinations of retardation wave plates and linear polarizers, both readily available at these wavelengths, allow for broadband spectral analysis. More recently, with increasing importance in vibrational circular dichroism, the demand for broadband circular polarization optics is shifting to mid-infrared and even terahertz frequencies [4, 5].

Therefore, many different chiral metamaterial designs have been proposed and realized experimentally over the past decade [6]. The vast majority of these designs is based on stacking multiple achiral layers with varying lateral orientation or composition, thus breaking mirror symmetry but at the same time allowing for fabrication with conventional electron-beam lithography processes [7–11]. Operation of most of these designs, however, is based on single resonances, thus yielding only small bandwidths. Chiral photonic crystals, created, for example, via three-dimensional laser lithography, can also exhibit giant chiro-optical effects. While large extinction ratios even in dual-band operation have been achieved, the bandwidth of dielectric photonic crystals and metamateri-

***Corresponding Author: Johannes Kaschke:** Institute of Applied Physics, Karlsruhe Institute of Technology, 76128 Karlsruhe, Germany, E-mail: johannes.kaschke@kit.edu
Martin Wegener: Institute of Applied Physics, Karlsruhe Institute of Technology, 76128 Karlsruhe, Germany

als is relatively low and a limiting factor for possible applications [12–17].

Helical metamaterials, based on periodic arrays of metallic helices, were the very first metamaterial design to exhibit both a large operation bandwidth and at the same time strong circular dichroism, making them ideal as broadband circular polarizers [18]. Recently, crystal growth theories and the synthesis of aperiodic ensembles of helical nanostructures have been reviewed [19, 20]. In this review article, we examine the principle of operation of helical metamaterials, that is, periodic arrays of helical nanostructures, and explore optimized designs that have been introduced over the past years. Furthermore, we also give an extensive overview over the different fabrication approaches, where we extend the discussion to self-assembly approaches yielding aperiodic ensembles. Finally, we review possible applications of helical metamaterials beyond the obvious far-field circular polarizer.

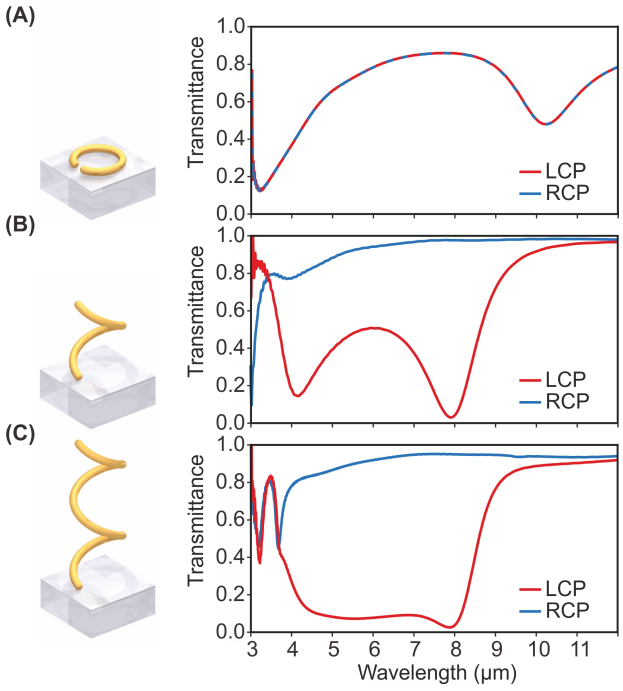

Figure 1: The three panels show the circular polarization normal-incidence transmittance spectra for the three different cases of an achiral split-ring resonator (A), a helix with one pitch (B), and a helix with two pitches as indicated on the left (C). For the achiral case in (A), transmittance for RCP and LCP is equal. Two distinct resonances with strong circular dichroism appears for a helix with one pitch, compared to the broad operation band for a helix with two pitches (C) (adapted with permission from [18]. Copyright 2009 American Association for the Advancement of Science).

2 Helical metamaterials and optimized designs

The basic principle of operation of helical metamaterials can be understood intuitively by considering the well-known split-ring resonator (SRR), one of the most widely known metamaterial building blocks. A unit cell with a single SRR, of course, is achiral under normal incidence of light, as there exists a plane of mirror symmetry and, therefore, transmittances for LCP and RCP are identical. If one, on the other hand, picks up one end of this SRR and moves it up in space, one creates a helix that has one axial pitch. As the mirror symmetry is now broken, a chiral unit cell has been created with the consequence of chiro-optical effects. Gansel et al. have first shown this in 2009 and corresponding numerical calculations are depicted in Figure 1 [18].

In the top panel, the transmittances for the case of a unit cell with a single SRR is shown. Transmittances for RCP and LCP are identical, as expected. Furthermore, two distinct resonances can be identified, corresponding to an “electric” and “magnetic” mode for linearly polarized light [21]. By moving one end of the SRR up in space, one creates a helix with one pitch. Only light with the corresponding circular polarization, for example, LCP for a left-handed helix, couples to this helix and is reflected. The other circular polarization, however, is transmitted. Figure 1(c) demonstrates that by increasing the number of pitches to merely two, a broad polarization band with a bandwidth of more than one octave is achieved. Helical metamaterials with more than one pitch can thus be seen as the analog to the common wire-grid polarizer for linear polarization. Optimized geometrical parameters have been discussed for these conventional helical metamaterials in detail through numerical calculations [22, 23].

When searching for an improved design that yields a larger bandwidth or a higher extinction ratio, nature delivers one inspiring and prominent example, namely, the DNA double helix. By intertwining two helices within one unit cell, Yang et al. showed in 2010 numerically that the performance of helical metamaterials based on gold or aluminum double helices can be improved considerably [24, 25]. This design, depicted in Figure 2(a), leads to a strong increase in bandwidth with a slightly decreased average extinction ratio though.

To circumvent this trade-off, a different approach to increasing the bandwidth was introduced by Gansel et al. in 2012 where the helix radius was tapered along the helix axis as depicted in Figure 2(b) [26]. The bandwidth in this design was enlarged to values of approximately 1.5 octaves. At the same time, the extinction ratio was improved.

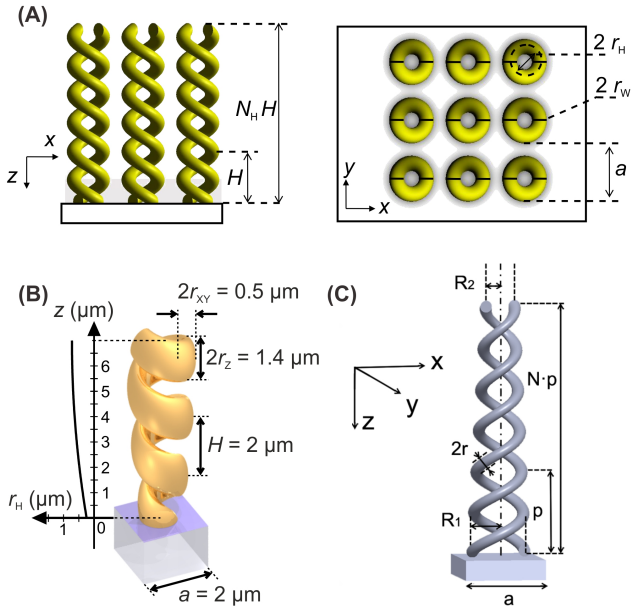

Figure 2: (A) Illustration of the optimized double-helix design (reprinted with permission from [24]. Copyright 2012 OSA). (B) Illustration of a tapered helical design that increases both, bandwidth and extinction ratio (adapted with permission from [26]. Copyright 2012 AIP Publishing LLC). (C) Combining the ideas of (B) and (C) yields a tapered double-helix design (reprinted with permission from [27]. Copyright 2012 IEEE).

Care must, however, be taken, as this design is not invariant with regard to the direction of propagation. Thus, owing to inherent circular polarization conversions, the transmittance spectra for incoming circular polarization are different depending on the direction from which light impinges, making the design for a certain orientation optimal as either a circular polarizer or a circular analyzer.

The optimized designs described earlier, namely, intertwining two helices within one unit cell and tapering the helix radius along the helix axis, can also be combined to yield a tapered double helix, introduced by Zhao et al. as depicted in Figure 2(c) [27]. Here, extinction ratio and bandwidth were improved simultaneously as well.

While all of these designs improve two key figures, namely, bandwidth and extinction ratio, they often exhibit unwanted circular polarization conversions, an aspect we have mentioned only in passing so far. Single-helix and double-helix designs inherently break rotational symmetry and thus exhibit linear birefringence. In turn, this causes nonvanishing off-diagonal elements of the Jones transmission matrix in circular polarization basis [28]. In 2011, Yang et al. proposed the idea of intertwining not only two, but three or four helices within a unit cell, further improving bandwidth and extinction ratio, but most of all, decreasing circular polarization by two orders of magnitude [29–31]. The design is illustrated in Figure 3(a). The constituent metal used in these calculations was aluminum. This choice is in contrast to most other metamaterial designs where noble metals normally yield the best results, due to small losses. For this design, however, losses are crucial. The necessity of losses in the system can be explained by a simple discussion exploiting symmetry arguments [32, 33]. In fact, by recovering threefold or fourfold rotational symmetry, one eliminates circular polarization conversions, as illustrated in Figure 3(b). Unfortunately, conversions are not eliminated solely in transmission but also in reflection. In reflection, on the other hand, the diagonal elements of the Jones matrix are generally equal because of reciprocity reasoning [33]. Therefore, for these so-called N-helical metamaterials where circular polarization conversions are eliminated, the reflectance spectra for both circular polarizations are equal and the undesired polarization cannot simply be reflected. Any difference in the circular transmittances must thus be due to a difference in absorption.

While N-helical metamaterials eliminate circular polarization conversions and yield previously unmatched bandwidths, the extinction ratio is much lower, because of the different principle of operation. By decreasing, for example, the helix radius, the extinction ratio can be increased, however, at the cost of a decreased bandwidth. Tapered $N = 3$ helices simultaneously lead to an increased extinction ratio and increased bandwidth of up to values of more than two octaves [33]. The numerically calculated data are depicted in Figure 3(c).

3 Micro- and nanofabrication of helical metamaterials

Metallic helical metamaterials for operation at visible or infrared frequencies pose a great challenge at the employed fabrication methods. Many conventional fabrication techniques used for the majority of two-dimensional metamaterials, such as electron-beam lithography, for example, are not ideal for helical designs. Nevertheless, a number of experimental approaches have emerged over the past decade. In the following, we discuss the four most prominent methods, namely, fabrication based on direct laser writing (DLW), focused-ion-beam induced deposition (FIBID), deposition at a glancing angle, as well as self-assembly approaches.

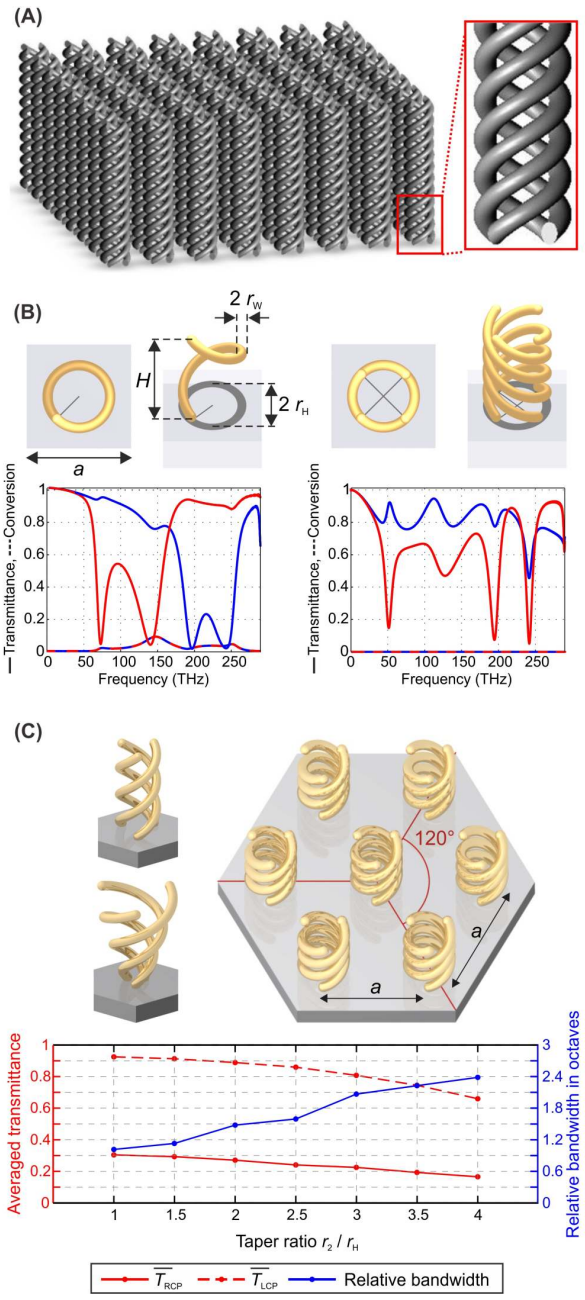

Figure 3: (A) First proposed design with four intertwined aluminum helices (reprinted with permission from [29]. Copyright 2011 OSA). (B) Illustration of single and $N = 4$-helices with corresponding numerically calculated transmittance spectra. While conversions (dashed lines) are eliminated in the latter case and the bandwidth is increased, the extinction ratio is strongly deteriorated (adapted with permission from [32]. Copyright 2012 OSA). (C) By arranging $N = 3$-helices in a hexagonal lattice, circular polarization conversions can also be eliminated. By furthermore tapering the helix radius, bandwidth and extinction ratio can be optimized simultaneously, as depicted in the bottom panel (adapted with permission from [33]. Copyright 2014 OSA).

3.1 Direct laser writing

DLW is a versatile tool to create almost arbitrary three-dimensional polymer structures at a submicrometer scale by strongly focusing a pulsed near-infrared laser into a sensitized photoresist [34–36]. Owing to a nonlinear absorption process, polymerization will only be initiated within the focal volume of the laser. By then moving the relative position of sample and laser focus, the desired polymer structure can be created. Chiral photonic crystals, both for visible and infrared frequencies, have been fabricated with DLW [12–15]. For helical metamaterials, however, DLW itself can only serve to create a polymer template. A more complex process including metal deposition is needed. The Wegener group introduced the solution to this problem in 2009 by combining direct laser writing in a positive-tone photoresist with subsequent electrochemical deposition of gold [18]. The method is illustrated in Figure 4(a). In the first step, an indium-tin-oxide (ITO) covered glass substrate is spin coated with a positive-tone photoresist. DLW is used to yield helical voids within the resist after development. These voids are filled with gold via electrochemical deposition. The ITO layer serves as the deposition cathode but will not be hindering in later applications, as it is transparent. In the final step, the residual photoresist is removed in an oxygen plasma, yielding, for example, gold structures as depicted in Figure 4(b). The left panel depicts an intermediate step, where the polymer template already containing gold helices that have been cut open via focused-ion-beam milling. The corresponding transmittance measurements are depicted in Figure 4(c). Strong circular dichroism is observed over a large bandwidth of approximately one octave.

Using the same approach, tapered helices can also be created, as depicted in Figure 4(d). As mentioned in the previous section, transmittance spectra will be different for forward and backward propagation. The corresponding experimental data, underline this point neatly. One would choose the orientation in the left panel for the use as an analyzer, as here the discrimination between circular polarizations is much more pronounced. For the use as a polarizer, the orientation as depicted on the right is favorable, as it leads to a higher degree of polarization for the transmitted light (not shown here).

The fabrication of nontapered and tapered helices has been demonstrated successfully with the process described earlier. *N*-Helical metamaterials for operation at visible or infrared frequencies, on the other hand, are not feasible by conventional DLW, as the resolution is limited by diffraction [37]. More importantly, the resolution of positive-tone photoresists is often also a further limit-

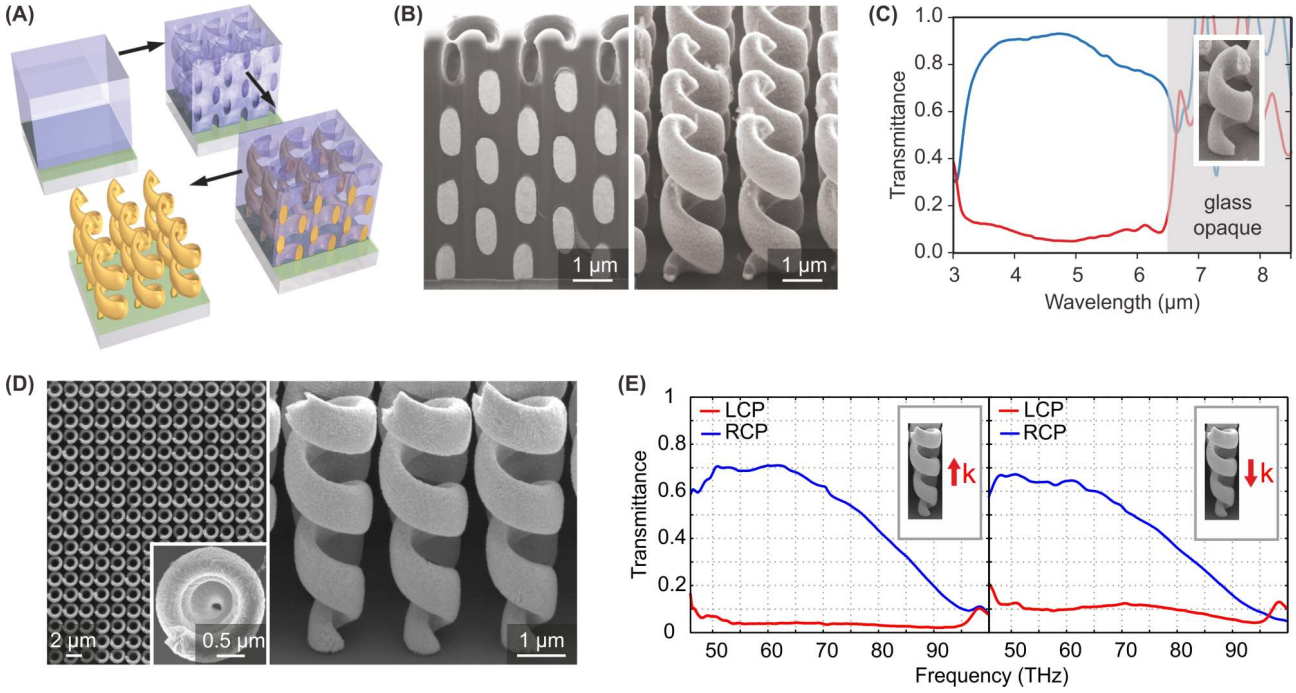

Figure 4: (A) The three major steps during fabrication via conventional direct laser writing in a positive-tone photo resist are illustrated. In a first step, voids are created with DLW in a spin-coated positive-tone photo-resist layer. Subsequently, the voids are filled with gold employing electrochemical deposition. In a final step, the photo resist template is removed via oxygen plasma etching. (B) Scanning electron micrographs of gold helical metamaterials, both before and after oxygen plasma etching. (C) Experimental transmittance spectra of the array depicted in (B). Incident circular polarizations LCP and RCP are color-coded by red and blue curves, respectively (A-C adapted with permission from [18]. Copyright 2009 American Association for the Advancement of Science). (D) Scanning electron micrographs of tapered helical metamaterials, also fabricated by the method depicted in (A). (E) Corresponding circular polarization transmittance spectra for both directions of propagation (D-E adapted with permission from [26]. Copyright 2012 AIP Publishing LLC).

ing factor. In order to achieve the necessary axial resolution needed to intertwine multiple helices within one unit cell, stimulation-emission-depletion inspired direct laser writing (STED-DLW) seems to be a suitable tool [37, 38]. The drawback, however, is the lack of an available positive-tone photoresist for STED-DLW. Thus, a similar approach has been introduced where, by STED-DLW, instead of voids a polymer shell was created in a first lithography step [39]. Followed by electrochemical deposition and oxygen-plasma etching, as in the process above, gold $N = 3$ helical metamaterials have been fabricated. Figure 5(a) depicts two scanning electron micrographs of the polymer template before electrochemical deposition and of the final gold structures, respectively. The definitive improvement in the axial resolution becomes evident by comparison to previously fabricated helical metamaterials.

Furthermore, all entries of the Jones transmission and reflection matrices in circular polarization basis were measured. The spectra were in good agreement with numerical calculations and expectations from symmetry-based theory, as depicted in Figure 5(b) [39]. Polarization conversions were successfully reduced to the order of measurement artifacts.

In passing, we mention another very different approach based on DLW that has been introduced [40]. Polymer double helices were created via single-shot exposure with a correspondingly shaped exposure focus. Subsequently, the entire sample was metallized with physical vapor deposition yielding a double-helical metamaterial. However, the underlying substrate is metallized as well and operation is, therefore, only possible in reflection with, thus, very limited application.

While DLW offers great freedom in the choice of the three-dimensional design and, in combination with electrochemical deposition, yields high-quality gold structures, the resolution is limited by diffraction laws. STED-DLW does yield an improvement in resolution and has allowed for the fabrication of more complex helical metamaterials. Nonetheless, operation at near-infrared or even visible frequencies is presently out of reach.

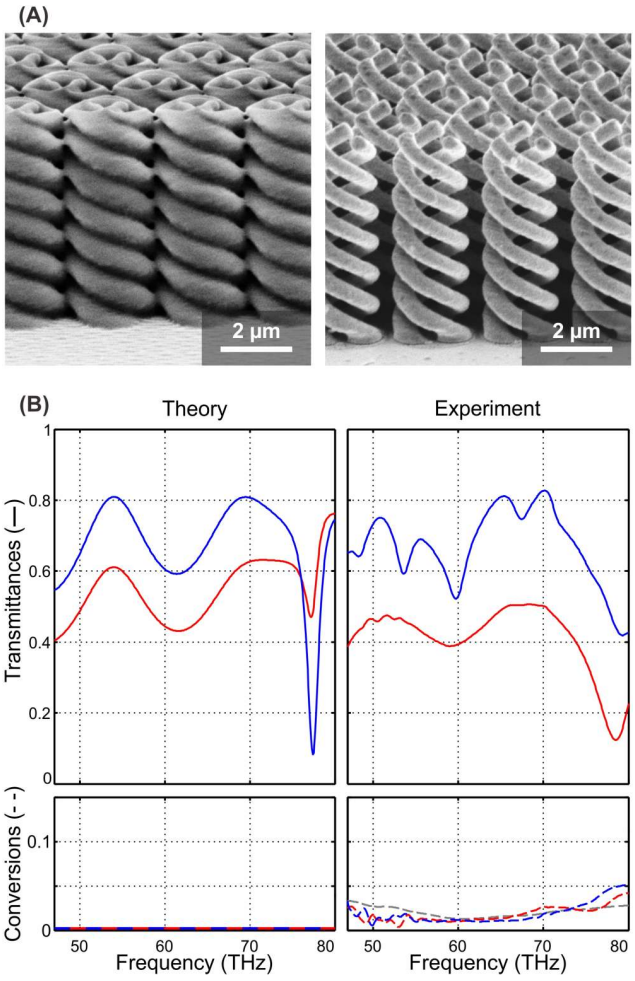

Figure 5: (A) Scanning electron micrographs of a polymer tem-plate for $N = 3$ helices fabricated via diffraction-unlimited STED-inspired direct laser writing on the left and the final gold structures after electrochemical gold deposition and removal of the polymer template on the right. (B) Corresponding numerical calculations and experimental transmission data are shown. The top panels depict the polarization-conserving transmittances. In the bottom panels circular polarization conversions are shown. It is evident that these have been reduced to a degree where they cannot be distinguished from measurement artifacts depicted by the dashed grey line (adapted with permission from [39]. Copyright 2015 OSA).

3.2 Focused-ion-beam induced deposition

An alternative promising method for fabricating three-dimensional metallic metamaterials is decomposition of a gaseous precursor initiated by either a focused electron beam or a focused ion beam [41, 42]. As the basic principle of (FIBID) and focused-electron-beam induced deposition (FEBID) is very similar, we mainly limit our discussion to the former in this review. Both methods, however, have been used successfully for the fabrication of helical metamaterials [43].

The principle of FIBID is illustrated in Figure 6(a). An ion beam is focused onto a substrate covered with a platinum-based precursor. Owing to surface-charge effects, bare glass substrates cannot be used. Fabrication has been demonstrated on silicon and gallium-nitride covered sapphire substrates, with the latter being transparent at visible frequencies and, thus, favorable for applications. The decomposition of the precursor leads to deposition of solid platinum on the substrate. By slowly moving the position of the ion beam such that the subsequent exposure volume has an overlap with previously deposited material, three-dimensional structures can be created. Therefore, FIBID and FEBID are slightly more limited in the choice of the geometry in comparison to DLW, as horizontal elements are inherently not possible. For most helical-metamaterial designs, this is not a limiting factor though. Advantageous, on the other hand, is the enhanced resolution making feature sizes well below 100 nm and lattice constants for helical metamaterials down to 400 nm possible [43].

The bottom panel of Figure 6(a) depicts scanning electron micrographs of platinum helical metamaterials fabricated via FIBID on a silicon substrate. By adjusting the exposure dose with increasing vertical position, up to five vertical pitches have been fabricated, unmatched by any other fabrication method.

Owing to the complex interactions of ion beam, precursor, substrate, and already deposited nanostructure, deposition parameters have to be adjusted empirically to yield optimal structure quality. These deposition parameters, however, lead to a deteriorated composition of the constituent material, that is, an increase in carbon concentration and a decrease in platinum concentration [43]. This in turn can lead to an inferior optical performance. Furthermore, one must note that the generally slow deposition speed on the order of tens of nanometers per second is reduced even further, because of local pressure reduction of the precursor. Therefore, for large-scale arrays, the so-called “refresh times” on the order of minutes have to be introduced after each individual helix to allow for precursor diffusion.

More recently, by exposing not an entire helix successively but only one-thirds of a pitch at a time, triple-helical metamaterials have been fabricated via FIBID [45]. The principle is illustrated in Figure 6(b). This method can be extended to any arbitrary number of intertwined helices, limited only by the resolution. The bottom-left panel of Figure 6(b) shows a scanning electron micrograph of an array of platinum triple helices on a sapphire substrate covered with AlGaN/GaN.

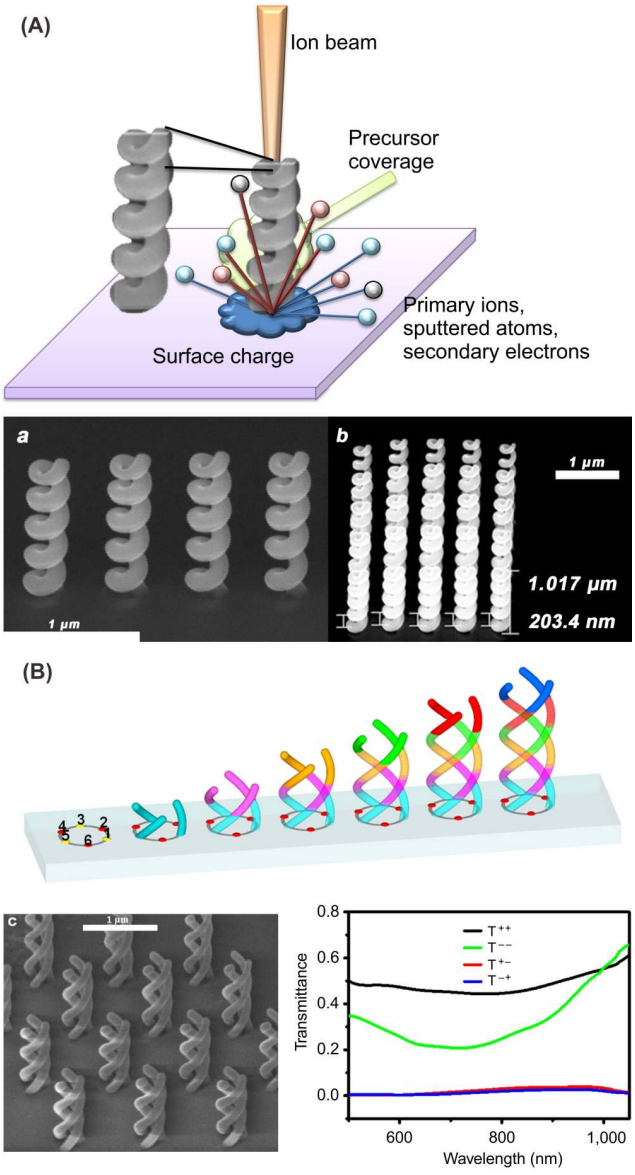

Figure 6: (A) The FIBID fabrication process is depicted schematically in the top panel. The bottom two panels depict scanning electron micrographs of arrays of platinum helices (reprinted with permission from [44]. Copyright 2013 John Wiley and Sons). (B) Tomographic rotatory growth is shown schematically in the top panel, allowing the fabrication of triple-helical nanostructures with FIBID. In the bottom panels, corresponding scanning electron micrographs (left) and transmittance spectra (right) of platinum triple-helical metamaterials are depicted. The scale bar corresponds to one micron (reprinted with permission from [45]. Copyright 2015 Nature Publishing Group).

While structure quality and periodicity are superb, one must note that the underlying quadratic translational lattice does not have the same rotational symmetry as the threefold rotationally invariant triple helix. Therefore, a reduction in circular polarization conversions but no complete elimination is expected, as observed previously for macroscopic samples at microwave frequencies [46]. The experimental transmission data are shown in the bottom-right panel of Figure 6(b). Strong circular dichroism is evident for wavelengths from approximately 500 to 1000 nm. Higher diffracted orders other than the zeroth orders will be present at these wavelengths though, because of the lattice period of 700 nm and the high refractive index of the supporting substrate.

FIBID is a promising candidate for future fabrication of complex helical metamaterials. While resolution and design freedom are two distinct advantages, slow writing speeds, the need for high-index substrates, and, most of all, inferior metal quality are the downside.

3.3 Glancing-angle deposition

While both, DLW and FIBID, offer great design freedom, fabrication of metamaterials on large-scale areas is out of reach. Parallelization of the fabrication can, for example, be achieved by physical vapor deposition under a glancing angle. With this technique, porous films and metamaterials can be fabricated with feature sizes below 100 nm. At the same time, the fabrication speed is increased by many orders of magnitude, as areas corresponding to the entire supporting wafer or substrate can be structured simultaneously.

Glancing-angle deposition (GLAD) is based on inhomogeneous nucleation and, subsequently, a shadowing effect for physical vapor deposition under an oblique angle [47]. When rotating the substrate during evaporation, helical structures are formed. Furthermore, by structuring the template prior to GLAD, for example, via electron-beam lithography, growth can be restricted to certain periodic points on the substrate leading to an improved periodicity and structural quality. Until recently, however, GLAD was limited to dielectrics, as especially noble metals have high surface mobility, leading to atom diffusion and thus hindering the creation of complex three-dimensional structures [48].

The Ghosh group in 2013 circumvented this problem by first creating a dielectric helical template via GLAD, which was subsequently covered with gold or silver nanoparticles by physical vapor deposition under a small tilt angle [49]. The process is illustrated in Figure 7(a). The scanning electron micrographs on the right show the dielectric helical template before and after silver evaporation. owing to self-shadowing and diffusion of the deposited metal atoms, no film of metal but isolated small metal islands are created. This leads to a strong

chiro-optical response that can be further increased by increasing the thickness of the silver nanoparticles. On the downside, the overall transmittance will successively decrease and scattering losses because of randomly distributed metal nanoparticles are to be expected.

The Fischer group tackled the direct deposition of noble metals by cooling the supporting substrate to a temperature of 170 K and thus hindering atom diffusion [48, 50]. Furthermore, prior to GLAD, a self-assembly-based process was used, in order to create periodically placed gold nanoparticles (AuNPs) with controllable size on the substrate. Therefore, structuring with time-consuming electron-beam lithography is needless. An illustration of the structured wafer, together with a corresponding scanning electron micrograph is depicted in Figure 7(b). Subsequently, by varying the composition of the evaporation flux, complex three-dimensional composite structures consisting up to three different materials were created. For optical applications, the simple gold helix design, as depicted in the left panel of Figure 7(c) was examined in detail.

The insets shown in the right panel of Figure 7(c) are transmission electron micrographs of the solid gold helices with two pitches, after they have been removed from the supporting substrate and suspended in aqueous solution. The corresponding transmission measurements show strong circular dichroism at visible frequencies, despite the random spatial orientation of the helices. The bandwidth, on the other hand, is well below one octave.

The chiro-optical response can furthermore be tuned very finely by not only changing the constituent metal but by even depositing alloys. Figure 7(c) shows a scanning electron micrograph of silver–copper alloy helices before removal from the supporting substrate. Circular dichroism spectra for these helices have also been examined for periodic arrays supported on glass substrates [50]. However, one must note that in this case, unwanted circular polarization conversions will again play a role and diminish the achievable extinction ratio. Similarly, the Zhao group has recently reported the fabrication of titanium–silver composite helices via GLAD [51].

In conclusion, glancing angle deposition has been shown to produce high-quality metal helices with feature sizes on the order of tenth of nanometers, bringing circular dichroism to visible frequencies. Owing to the parallel fabrication approach on the entire substrate or wafer, fabrication speeds surpass those of DLW, FIBID, and FEBID by many orders of magnitude. Slightly more complex designs and even the fabrication of composite structures consisting of more than one metal have been demonstrated.

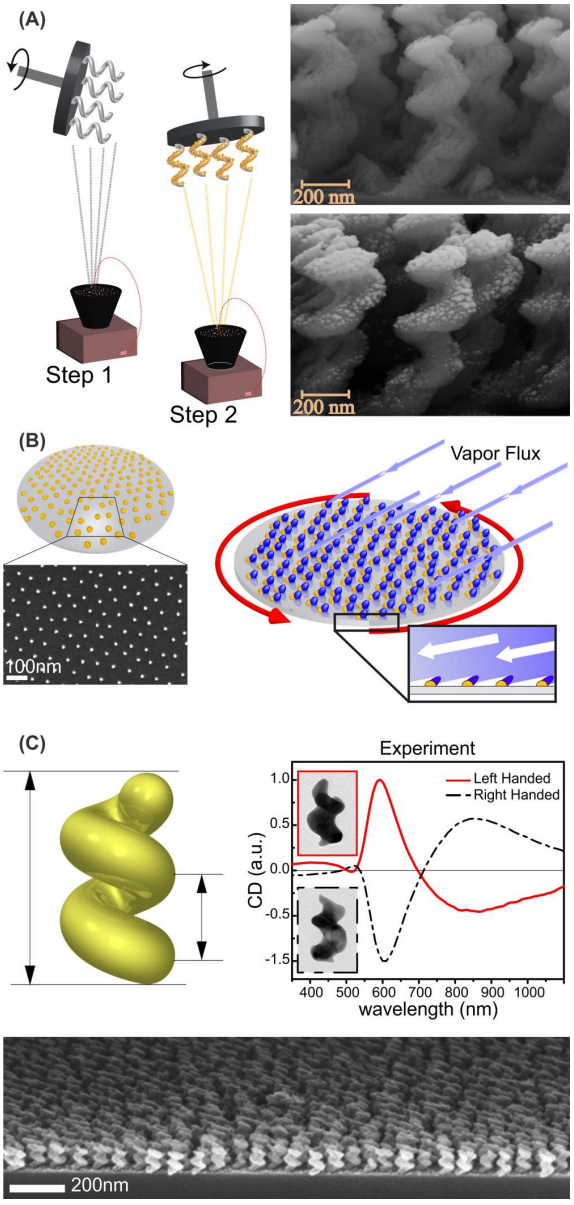

Figure 7: (A) Schematics of hybrid GLAD approach (left). Under a glancing angle, silica helices are created as depicted in the scanning electron micrograph in the top-right. Afterwards, under a small tilt angle silver is deposited. The final structures are shown in the scanning electron micrograph in the bottom-right (reprinted with permission from [49]. Copyright 2013 Royal Society of Chemistry). (B) Illustration and scanning electron micrograph of a prestructured substrate with gold nanoparticles (left), as well as illustration of GLAD process (right). Scale bar corresponds to 100 nm. (C) Blueprint of the helical gold structure (left). Experimental circular dichroism spectra for left- and right-handed helices in solution are depicted on the right with corresponding transmission electron micrographs as insets. The scanning electron micrograph in the bottom panel depicts an array of silver-copper alloy helices before release to solution (B-C reprinted with permission from [48]. Copyright 2013 Nature Publishing Group).

For compact periodic helical metamaterials, GLAD approaches will always yield linear birefringence and thus circular polarization conversions. Furthermore, complex designs, as intertwined helices or super lattices, for example, are inherently not possible with GLAD.

A related approach that we mention here in passing is also based on the fabrication of chiral metamaterials via metal evaporation under a glancing angle. In this method, named "repetitive hole-mask colloidal lithography," an evaporation mask is generated via drop casting of polystyrene nanospheres and subsequent gold evaporation [52]. Through this mask, large areas of randomly distributed nanostructures similar two half-pitch helices have been fabricated by rotating the substrate during physical vapor deposition under a tilt angle. By repeating the procedure for different rotation angles, linear birefringence and thus circular polarization conversions can furthermore be eliminated. Truly three-dimensional structures are, nonetheless, out of reach for this approach, leading to comparably small amplitudes of the circular dichroism signal.

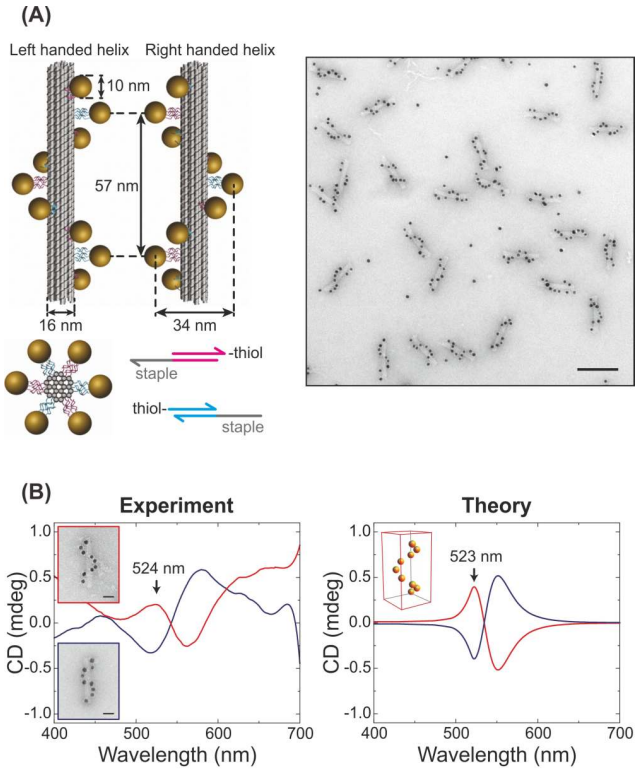

Figure 8: (A) Schematic blueprint of self-assembled gold nanospheres on DNA bundles arranged as either left-handed or right-handed helix. The panel on the right depicts a transmission electron micrograph of an ensemble of left-handed helices. The scale bar corresponds to 100 nm. (B) Experimental circular dichroism spectra (left) for a left- and right-handed depicted in blue and in red, respectively. The corresponding numerical calculations are depicted on the right. (adapted with permission from [54]. Copyright 2012 Nature Publishing Group).

3.4 DNA-based self-assembly

Self-assembly techniques are unrivalled in resolution by any top-down approach and are thus attractive for creating metamaterials for operation at visible frequencies. Furthermore, as fabrication can be parallelized to a large extend, process times can be reduced considerably. For many years, however, self-assembly of metallic nanostructures has been limited to the fabrication of very simple designs. Over the past decade, however, molecular linking of plasmonic nanoparticles has allowed for the fabrication of nanostructures that are more complex and in particular DNA has emerged as a paradigm linker for more sophisticated designs [53].

DNA-based self-assembly has been used recently to fabricate helical nanostructures, schematically depicted in Figure 8(a) [54]. In the first step, DNA origami-folded helix bundles were created. AuNPs with a diameter of 10 nm were synthesized in solution and subsequently conjugated with thiolated single-stranded DNA (ssDNA) strands. These DNA-coated AuNPs were hybridized to the DNA origami structure, yielding either right-handed or left-handed helix formations of AuNPs.

The transmission electron micrograph in the right panel of Figure 8(a) shows an ensemble of left-handed helices. The experimental spectra, as well as corresponding numerical calculations, are depicted in Figure 8(b). Resonant circular dichroism is observed for wavelengths of approximately 520 nm. The amplitude of the circular dichroism signal is only on the order of millidegrees, however, and thus orders of magnitude smaller than for GLAD approaches. The optical performance can, however, be enhanced by electroless gold deposition. This step increases the sizes of the nanoparticles and leads to a small, expected red-shift of the peak, but mostly increases the amplitude of the signal by a factor of approximately 400 [54].

Furthermore, composite shells, consisting of an alloy of gold and silver, can also be created, yielding the possibility to finely tune the spectral position and the amplitude of the CD signal.

Nevertheless, helical nanostructures fabricated via DNA-based self-assembly show rather weak circular dichroism and small bandwidth, compared to the methods discussed in the previous paragraphs, resulting from the disconnected nanoparticle design. Furthermore, the formation of compact, periodic metamaterials is impossible.

For solution-based applications, however, DNA-based self-assembly is a promising method. Parallelized large-scale fabrication of more complex designs is fundamentally possible. Feature sizes presented so far are out of reach for top-down approaches such as DLW and FIBID and even challenging for GLAD.

The four most prominent methods, discussed earlier, are summarized in Table 1 together with the characteristic strengths and weaknesses. Furthermore, a typical spectral range at which operation has been demonstrated for the corresponding technique is given.

3.5 Hybrid fabrication approaches

Finally, we also point out some recently reported novel fabrication approaches for chiral metamaterials using electron-beam lithography. While no actual helical nanostructures have been reported yet, very similar chiral designs have been demonstrated.

Electron-beam lithography is a widely spread and well-defined process, but generally limited to the fabrication of two-dimensional layers. Recently, however, the so-called on-edge lithography has emerged [55]. The general principle consists of two steps: in the first step, the underlying substrate is topographically structured via wet etching or DLW. In the second step, electron-beam lithography, noble-metal evaporation, and a final lift-off process yield three-dimensional metallic nanostructures.

Dietrich et al. first introduced the process in 2012, where a silica substrate was structured with long trenches, on sides of which arrays of three-dimensional L-shaped structures were subsequently fabricated [55]. Strong circular dichroism was observed for wavelengths from 800 to 1,400 nm. However, because of the lack of rotational symmetry strong linear birefringence is to be expected. As described previously, this problem can be solved by recovering fourfold rotational symmetry, as was done shortly after [56]. Here, starfish-shaped metallic nanostructures were written on top of a conical topography, a structure distantly related to tapered 4-helices. The obtained bandwidth was rather small, opposed to the large bandwidths tapered N-helices normally yield.

A different approach for structuring the underlying substrate via DLW prior to electron-beam lithography has also been presented. Even though no chiral metamaterials have been fabricated, it is evident that, despite the limited resolution of DLW, more complex topographies are possible [57]. Especially tapered helical metamaterials with few pitches could, therefore, be fabricated via on-edge lithography in the near future.

4 Applications beyond far-field circular polarizers

For most of the literature, helical metamaterials, or in fact chiral metamaterials in general, have been discussed as paradigms for (broadband) circular polarizers. Similarly, in combination with opaque substrates, helical metamaterials have been proposed as perfect, broadband absorbers [58].

For individual helical metallic nanostructures, other groundbreaking applications such as magnetic micromachines with the possible task of localized drug delivery have emerged [59]. Here, we focus on examples of possible other applications of ordered helical metamaterials extending beyond the simple circular polarizer.

4.1 Circular polarization converter

One interesting aspect of chiral metamaterials is the possibility of the so-called asymmetric transmission, a difference in transmittance for a certain polarization depending on the direction of propagation [60, 61]. In fact, for all reciprocal materials and excluding any nonlinear effects, the Jones matrix in backward propagation direction corresponds to the transpose of the Jones transmission direction in forward direction [62]. Therefore, polarization-conserving transmittances, that is, the diagonal elements of the Jones transmission matrix, are identical for forward and backward propagation. A difference in the polarization conversions, however, results in an asymmetric Jones transmission matrix and thus in a difference in transmittance for a certain polarization depending on the direction of propagation. Therefore, by strongly increasing one of the polarization conversions and suppressing all other elements of the Jones matrix, strong asymmetric transmission can be achieved.

For circularly polarized light, such efficient polarization converters have long been limited in bandwidth or efficiency [63, 64]. Recently, a novel design based on helical metamaterials has been introduced [65]. The design consists of two gold helices with opposing handedness connected by a small arc as depicted in Figure 9(a). The adjacent scanning electron micrograph shows an array these complex gold structures fabricated via diffraction-unlimited direct laser writing.

We recall that circularly polarized light couples only to a helix of matching handedness in which case it is reflected. In contrast to what one might assume intuitively, the presented design does not block both circular polar-

Table 1: Summary of experimental approaches for fabricating metallic helical metamaterials Four methods have been successfully employed to fabricate metallic helical metamaterials for operation at visible and infrared frequencies. The table above lists corresponding publications, as well as strengths and weaknesses of each approach.

Method	Publications	Spectral range	Advantages	Disadvantages
DLW/ STED-DLW	Wegener group [18, 26, 39, 65]	Mid-infrared	high metal quality highest degree of design freedom	limited resolution low writing speeds
FIBID/ FEBID	Passaseo group [43–45]	Near-infrared	improved resolution large design freedom	low metal quality low writing speeds
GLAD	Ghosh group [49] Fischer group [48, 50] Zhao group [51]	Visible	small feature sizes fabrication of composites wafer-scale fabrication	low structural quality small bandwidths limited design freedom
DNA-based self-assembly	Liedl group [54]	Visible	small feature sizes scalable fabrication volumes	small chiro-optical response narrow bandwidths no ordered media

izations but, instead, exhibits strong circular polarization conversions for one circular polarization. This effect was explained by an analysis of the current distributions under excitation with circular polarization. When the circular polarization matches the handedness of the helix it first impinges on, large currents are only observed in that first helix. If, however, the circular polarization matches that of the second helix, because of coupling, large currents will be observed in both helices. The four elements of the Jones transmission matrix in circular polarization basis were measured and compared to numerical calculations, as depicted in Figure 9(b). Strong circular polarization conversions from RCP to LCP were achieved over a large bandwidth of approximately one octave, while the other elements of the Jones matrix were strongly suppressed, all in very good agreement with theory.

4.2 Chiral near-field sources

Recently, *N*-helical metamaterials have been proposed to serve as chiral near-field sources [66]. Here, the helices are not excited by circularly polarized but linearly polarized light, propagating in a direction orthogonal to the helix axis as depicted in Figure 10(a). The induced currents in the helices lead to a magnetic field in the enclosed volume that is either parallel or antiparallel to the electric field, depending on the handedness of the helices. By locally calculating the normalized optical activity, the authors demonstrated that strong chiral near fields are induced within the helical volume, as depicted in Figure 10(b). The geometrical parameters chosen in this case are, however, out of reach for direct laser writing and even for FIBID. A scaled-up design with a pitch of two micrometer was also presented, leading to a slight decrease in the normalized local optical chirality by a factor of 1.7.

A large local optical chirality is not sufficient, however, for the application in chiro-optical spectroscopy. In order to get a measure for the possible enhancement in circular dichroism measurements, the normalized optical activity needs to be averaged over a certain volume in which the analyte, for example, chiral biological molecules, will be dispersed. Comparing this value to the far-field differential circular dichroism signal gives a measure of the possible enhancement in signal amplitude. As depicted in Figure 10(c), strong enhancement can be achieved with values of up to 80-fold.

5 Conclusions and Outlook

Helical metamaterials have been a vibrant field of research over the past years and have evolved from a paradigm as broadband circular polarizers to more complex geometrical designs with novel applications. Simple geometrical alterations have allowed for enhanced optical performance. With *N*-helical metamaterials, previously inherent circular polarization conversions have been eliminated and operation bandwidths have been increased to previously unmatched values.

Simultaneously, the complexity has been increasing steadily, thus also posing a demand for more advanced micro- and nanofabrication techniques. We have reviewed the recent advances in laser lithography and FIBID. Both

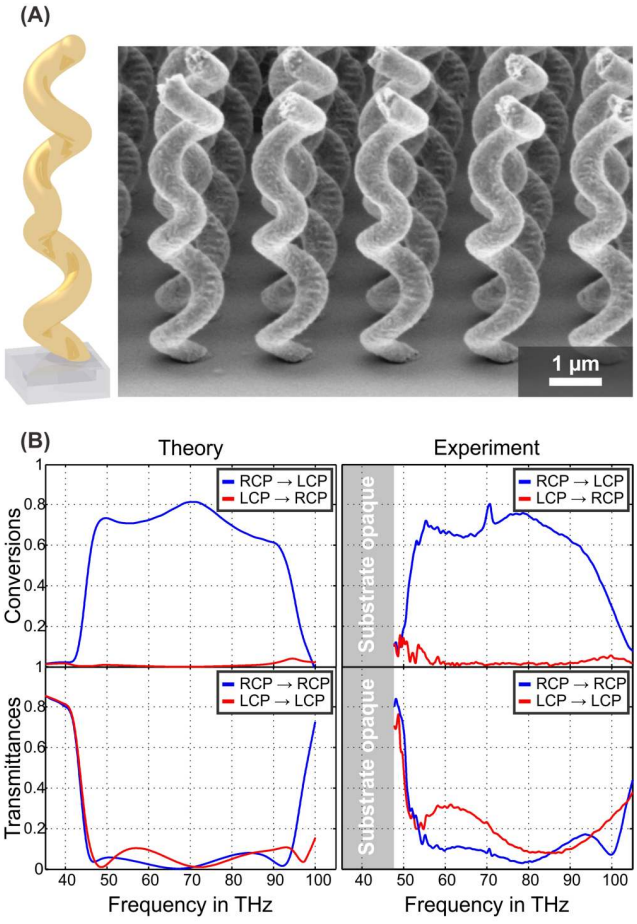

Figure 9: (A) Illustration of the circular polarization converter design. A left-handed gold helix on the top is followed by a right-handed gold helix, each of which has 1.5 pitches. The scanning electron micrograph on the right depicts an array fabricated via STED-inspired direct laser writing. (B) Numerical calculations and experimental data for all four entries of the Jones matrix in circular polarization basis. Polarization conversions are depicted in the top, polarization-conserving transmittances in the bottom row (adapted with permission from [65]. Copyright 2015 John Wiley and Sons).

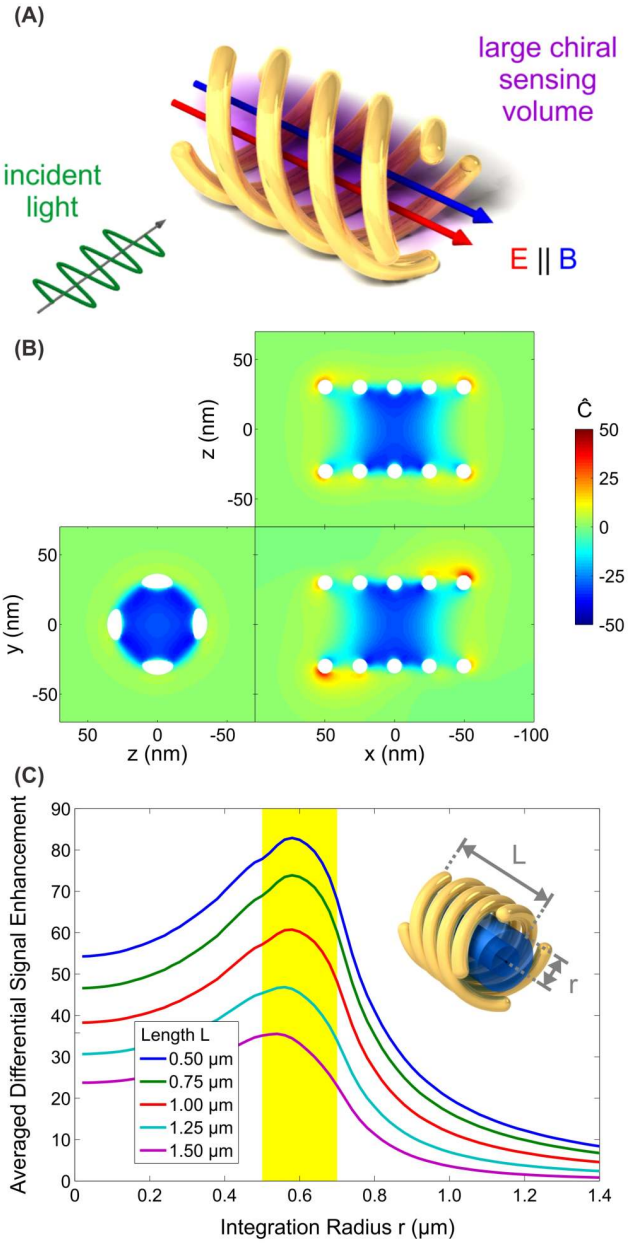

Figure 10: (A) Scheme of chiral near-field source: an $N = 4$-helix is excited by a linearly polarized field propagating in a direction orthogonal to the helix axis. (B) False color plots of the numerically calculated normalized optical chirality for the proposed geometrical parameters. (C) The averaged normalized optical activity is shown for an $N = 4$-helix with geometrical parameters that are achievable with DLW. The normalized optical activity was averaged over a cylindrical volume, defined by the length L and the cylindrical radius r, giving a measure for the enhancement of the chiro-optical response (reprinted with permission from [66]. Copyright 2014 American Chemical Society)

methods allow for the fabrication of highly complex three-dimensional metallic nanostructures for operation at mid- and near-infrared frequencies. On the other hand, fabrication techniques for wafer-scale fabrication have been introduced in the form of glancing-angle deposition and DNA-based self-assembly, bringing giant chiro-optical effects even to visible frequencies.

With an increasing number of novel applications that we have touched upon and the growing importance of vibrational circular dichroism spectroscopy, the field of helical metamaterials will remain an interesting research topic and will likely drive the development of new nano- and microfabrication approaches also in the future.

Acknowledgement: The authors acknowledge support by the Deutsche Forschungsgemeinschaft (DFG), Open Access Publishing Fund of Karlsruhe Institute of Technology,

the State of Baden-Wuerttemberg, and the Karlsruhe Institute of Technology (KIT) through the DFG-Center for Functional Nanostructures (CFN) within subprojects A1.4 and A1.5. The Ph.D. education of J.K. is embedded in the Karlsruhe School of Optics & Photonics (KSOP).

References

[1] Fleury R, Monticone F, Alu A. Invisibility and cloaking: Origins, present, and future perspectives. Phys Rev Appl 2015, 4, 037001.
[2] Soukoulis CM, Wegener M. Past achievements and future challenges in the development of three-dimensional photonic metamaterials. Nature Photon 2011, 5, 523–530.
[3] Beychok S. Circular dichroism of biological macromolecules. Science 1966, 154, 1288–1299.
[4] Singh RD, Keiderling TA. Vibrational circular dichroism of poly(γ-benzyl-l-glutamate). Biopolymers 1981, 20, 237–240.
[5] Choi JH, Cho M. Terahertz chiroptical spectroscopy of an a-helical polypeptide: A molecular dynamics simulation study. J Phys Chem B 2014, 118, 12837–12843.
[6] Valev VK, Baumberg JJ, Sibilia C, Verbiest T. Chirality and chiroptical effects in plasmonic nanostructures: Fundamentals, recent progress, and outlook. Adv Mater 2013, 25, 2517–2534.
[7] Liu N, Liu H, Zhu S, Giessen H, Stereometamaterials. Nature Photon 2009, 3, 157–162.
[8] Decker M, Ruther M, Kriegler CE, et al. Strong optical activity from twisted-cross photonic metamaterials. Opt Lett 2009, 34, 2501–2503.
[9] Decker M, Zhao R, Soukoulis CM, Linden S, Wegener M. Twisted split-ring-resonator photonic metamaterial with huge optical activity. Opt Lett 2010, 35, 1593–1595.
[10] Zhao Y, Belkin M, Alu A. Twisted optical metamaterials for planarized ultrathin broadband circular polarizers. Nat Commun 2012, 3, 870.
[11] Hentschel M, Schäferling M, Weiss T, Liu N, Giessen H. Three-dimensional chiral plasmonic oligomers. Nano Lett 2012, 12, 2542–2547.
[12] Thiel M, Decker M, Deubel M, Wegener M, Linden S, von Freymann G. Polarization stop bands in chiral polymeric three-dimensional photonic crystals. Adv Mater 2007, 19, 207–210.
[13] Thiel M, von Freymann G, Wegener M. Layer-by-layer three-dimensional chiral photonic crystals. Opt Lett 2007, 32, 2547–2549.
[14] Thiel M, Rill MS, von Freymann G, Wegener M. Three-dimensional bi-chiral photonic crystals. Adv Mater 2009, 21, 4680–4682.
[15] Thiel M, Ott J, Radke A, Kaschke J, Wegener M. Dip-in depletion optical lithography of three-dimensional chiral polarizers. Opt Lett 2013, 38, 4252–4255.
[16] Takahashi S, Tajiri T, Ota Y, Tatebayashi J, Iwamoto S, Arakawa Y. Circular dichroism in a three-dimensional semiconductor chiral photonic crystal. Appl Phys Lett 2014, 105, 051107.
[17] Chadha A S, Zhao D, Zhou W. Comparative study of metallic and dielectric helix photonic metamaterial. Optical Materials Express 2014, 4, 2460–2467.
[18] Gansel JK, Thiel M, Rill MS, et al. Gold helix photonic metamaterial as broadband circular polarizer. Science 2009, 325, 1513–1515.
[19] Liu L, Zhang L., Kim SM, Park S. Helical metallic micro- and nanostructures: fabrication and application. Nanoscale 2014, 6, 9355–9365.
[20] Ren Z, Gao PX. A review of helical nanostructures: growth theories, synthesis strategies and properties. Nanoscale 2014, 6, 9366–9400.
[21] Linden S, Enkrich C, Wegener M, Zhou J, Koschny T, Soukoulis CM. Magnetic response of metamaterials at 100 terahertz. Science 2004, 306, 1351–1353.
[22] Gansel JK, Wegener M, Burger S, Linden S. Gold helix photonic metamaterials: A numerical parameter study. Opt Express 2010, 18, 1059–1069.
[23] Wu L, Yang Z, Zhao M, et al. What makes single-helical metamaterials generate pure circularly polarized light. Opt Express 2012, 20, 1552–1560.
[24] Yang Z, Zhao M, Lu PX, Lu YF. Ultrabroadband optical circular polarizers consisting of double-helical nanowire structures. Opt Lett 2010, 35, 2588–2590.
[25] Yang Z, Zhao M, Lu YF. Similar structures, different characteristics: Optical performances of circular polarizers with single- and double-helical metamaterials. J Lightwave Technol 2010, 28, 3055–3061.
[26] Gansel JK, Latzel M, Frölich A, Kaschke J, Thiel M, Wegener M. Tapered gold-helix metamaterials as improved circular polarizers. Appl Phys Lett 2012, 100, 101109.
[27] Zhao Z, Gao D, Bao C, Zhou X, Lu T, Chen L. High extinction ratio circular polarizer with conical double-helical metamaterials. J Lightwave Technol 2012, 30, 2442–2446.
[28] Menzel C, Rockstuhl C, Lederer F. Advanced jones calculus for the classification of periodic metamaterials. Phys Rev A 2010, 82, 053811.
[29] Yang Z, Zhao M, Lu PX. Improving the signal-to-noise ratio for circular polarizers consisting of helical metamaterials. Opt Express 2011, 19, 4255–4260.
[30] Yang Z, Zhang P, Xie P, Wu L, Lu Z, Zhao M. Polarization properties in helical metamaterials. Frontiers of Optoelectronics 2012, 5, 248–255.
[31] Lu Z, Zhao M, Xie P, et al. Reflection properties of metallic helical metamaterials. J Lightwave Technol 2012, 30, 3050–3054.
[32] Kaschke J, Gansel JK, Wegener M. On metamaterial circular polarizers based on metal N-helices. Opt Express 2012, 20, 26012–26020.
[33] Kaschke J, Blome M, Burger S, Wegener M. Tapered N-helical metamaterials with three-fold rotational symmetry as improved circular polarizers. Opt Express 2014, 22, 19936–19946.
[34] Kawata S, Sun HB, Tanaka T, Takada K. Finer features for functional microdevices. Nature 2001, 412, 697–698.
[35] Straub M, Gu M. Near-infrared photonic crystals with higher-order bandgaps generated by two-photon photopolymerization. Opt Lett 2002, 27, 1824–1826.
[36] Deubel M, von Freymann G, Wegener M, Pereira S, Busch K, Soukoulis CM. Direct laser writing of three-dimensional photonic-crystal templates for telecommunications. Nat Mater 2004, 3, 444–447.
[37] Fischer J, Wegener M. Three-dimensional optical laser lithography beyond the diffraction limit. Laser Photon Rev 2013, 7, 22–44.

[38] Fischer J, Wegener M. Three-dimensional direct laser writing inspired by stimulated-emission-depletion microscopy. Opt Mater Exp 2011, 1, 614–624.
[39] Kaschke J, Wegener M. Gold triple-helix mid-infrared metamaterial by STED-inspired laser lithography. Opt Lett 2015, 40, 3986–3989.
[40] Zhang SJ, Li Y, Liu ZP, et al. Two-photon polymerization of a three dimensional structure using beams with orbital angular momentum. Appl Phys Lett 2014, 105, 061101.
[41] Matsui S, Kaito T, Fujita JI, Komuro M, Kanda K, Haruyama Y. Three-dimensional nanostructure fabrication by focused-ion-beam chemical vapor deposition. J Vac Sci Technol B 2000, 18, 3181–3184.
[42] Utke I, Hoffmann P, Melngailis J. Gas-assisted focused electron beam and ion beam processing and fabrication. J Vac Sci Technol B 2008, 26, 1197–1276.
[43] Esposito M, Tasco V, Cuscunŕ M, et al. Nanoscale 3D chiral plasmonic helices with circular dichroism at visible frequencies. ACS Photonics 2015, 2, 105–114.
[44] Esposito M, Tasco V, Todisco F, Benedetti A, Sanvitto D, Passaseo A. Three dimensional chiral metamaterial nanospirals in the visible range by vertically compensated focused ion beam induced-deposition. Adv Opt Mater 2014, 2, 154–161.
[45] Esposito M, Tasco V, Todisco F, et al. Triple-helical nanowires by tomographic rotatory growth for chiral photonics. Nat Commun 2015, 6, 6484.
[46] Zhang P, Yang Z, Zhao M, et al. Similar structures, different characteristics: circular dichroism of metallic helix arrays with single-, double-, and triple-helical structures. J Opt Soc Am A 2013, 30, 677–681.
[47] Ye DX, Karabacak T, Picu RC, Wang GC, Lu TM. Uniform Si nanostructures grown by oblique angle deposition with substrate swing rotation. Nanotechnology 2005, 16, 1717–1723.
[48] Mark AG, Gibbs JG, Lee TC, Fischer P. Hybrid nanocolloids with programmed three-dimensional shape and material composition. Nat Mater 2013, 12, 802–807.
[49] Singh JH, Nair G, Ghosh A, Ghosh A. Wafer scale fabrication of porous three-dimensional plasmonic metamaterials for the visible region: chiral and beyond. Nanoscale 2013, 5, 7224–7228.
[50] Gibbs JG, Mark AG, Eslami S, Fischer P. Plasmonic nanohelix metamaterials with tailorable giant circular dichroism. Appl Phys Lett 2013, 103, 213101.
[51] Larsen GK, He Y, Wang J, Zhao Y. Scalable fabrication of composite Ti/Ag plasmonic helices: Controlling morphology and optical activity by tailoring material properties. Adv Opt Mater 2014, 2, 245–249.
[52] Zhao J, Jaber S, Mulvaney P, Braun PV, Giessen H. Repetitive hole-mask colloidal lithography for the fabrication of large-area low-cost plasmonic multishape single-layer metasurfaces. Adv Opt Mater 2015, 3, 680–686.
[53] Tan SJ, Campolongo MJ, Luo D, Cheng W. Building plasmonic nanostructures with DNA. Nat Nanotechnol 2011, 6, 268–276.
[54] Kuzyk A, Schreiber R, Fan Z, et al. DNA-based self-assembly of chiral plasmonic nanostructures with tailored optical response. Nature 2012, 483, 311–314.
[55] Dietrich K, Lehr D, Helgert C, Tünnermann A, Kley EB. Circular dichroism from chiral nanomaterial fabricated by on-edge lithography. Adv Mater 2012, 24, OP321–OP325.
[56] Dietrich K, Menzel C, Lehr D, et al. Elevating optical activity: Efficient on-edge lithography of three-dimensional starfish metamaterial. Appl Phys Lett 2014, 104, 193107.
[57] Staude I, Decker M, Ventura MJ, et al. Hybrid high-resolution three-dimensional nanofabrication for metamaterials and nanoplasmonics. Adv Mater 2013, 25, 1259–1259.
[58] Lu Z, Zhao M, Yang Z, Wu L, Zhang P. Helical Metamaterial Absorbers: Broadband and Polarization-Independent in Optical Region. J Lightwave Technol 2013, 31, 2762–2768.
[59] Tottori S, Zhang L, Qiu F, Krawczyk KK, Franco-Obregón A, Nelson BJ. Magnetic Helical Micromachines: Fabrication, Controlled Swimming, and Cargo Transport. Adv Mater 2012, 24, 811–816.
[60] Menzel C, Helgert C, Rockstuhl C, et al. Asymmetric transmission of linearly polarized light at optical metamaterials. Phys Rev Lett 2010, 104, 253902.
[61] Grady NK, Heyes JE, Chowdhury DR, et al. Terahertz metamaterials for linear polarization conversion and anomalous refraction. Science 2013, 340, 1304–1307.
[62] Armitage NP. Constraints on jones transmission matrices from time-reversal invariance and discrete spatial symmetries. Phys Rev B 2014, 90, 035135.
[63] Wu C, Arju N, Kelp G, et al. Spectrally selective chiral silicon metasurfaces based on infrared fano resonances. Nat Commun 2014, 5, 3892.
[64] Pfeiffer C, Zhang C, Ray V, Guo LJ, Grbic A. High performance bianisotropic metasurfaces: Asymmetric transmission of light. Phys Rev Lett 2014, 113, 023902.
[65] Kaschke J, Blume L, Wu L, et al. A helical metamaterial for broadband circular polarization conversion. Adv Opt Mater 2015, 3, 1411–1417.
[66] Schäferling M, Yin X, Engheta N, Giessen H. Helical plasmonic nanostructures as prototypical chiral near-field sources. ACS Photonics 2014, 1, 530–537.